# Molecular-dynamics study of copper with defects under strain

P. Heino
*Laboratory of Computational Engineering, Helsinki University of Technology, Miestentie 3, P. O. Box 9400, FIN-02015 Espoo, Finland*

H. Häkkinen
*Department of Physics, University of Jyväskylä, P. O. Box 35, FIN-40351 Jyväskylä, Finland*

K. Kaski
*Laboratory of Computational Engineering, Helsinki University of Technology, Miestentie 3, P. O. Box 9400, FIN-02015 Espoo, Finland*
(Received 11 February 1998; revised manuscript received 31 March 1998)

Mechanical properties of copper with various types of defects have been studied with the molecular-dynamics method and the effective-medium theory potential both at room temperature and near zero temperature. The loading has been introduced as constant rate straining and the dynamics of the process region of fracture is purely Newtonian. With the model three types of defects were studied: point defects, grain boundary, and an initial void serving as a crack seed. Point defects were seen to decrease the system strength in terms of fracture stress, fracture strain, and elastic modulus. Due to random microstructure, highly disordered systems turned out to be isotropic, which on the other hand seems to increase the elastic modulus. In the case of a grain boundary, the elastic modulus was found to be significantly less than the bulk value of the system. In addition, the critical strain for crack initiation seems to be less at the grain boundary than in the bulk. In the case of an initial void, we studied stress concentration, dislocation propagation, and crack propagation in thin systems. The stress concentration was found to be in surprisingly good agreement with continuum predictions. Dislocation and crack were propagated with a velocity much below the speed of sound and they preferred the ⟨110⟩ crystal orientation. [S0163-1829(98)03826-0]

## I. INTRODUCTION

Recently, the dynamics of fracture has received considerable interest. From the physics point of view, fracture in solid materials involves processes on a wide range of length and time scales. Theoretically, different length scales can been treated with macroscopic continuum models,[1] mesoscopic spring models[2] or by using a truly microscopic approach with interatomic potential. Because in the atomistic case a realistic potential can be hard to find, approximate pair potentials are often used. For example, Morse,[3,4] Lennard-Jones (LJ) (Refs. 5 and 6), or Johnson[3,7] potentials are quite common. Holian *et al.*[5] have compared the Morse and LJ potentials with a more realistic many-body potential. They found that generally the pair potentials yield brittle behavior, while ductile materials must be described with a many-body potential. On the other hand, in dynamic fracture simulations large system sizes are necessary because of the boundary effects such as wave reflection and the problem of dislocations near fixed boundaries. Thus, simulations have so far mostly been done by using a simple pair potential in a two-dimensional system[6,7] or in a system with otherwise less degrees of freedom.[8] Until recently, three-dimensional (3D) simulations with a realistic many-body potential for describing the behavior of ductile materials, e.g., copper, could be realized only in small systems.[9,10] However, with the rapid development of parallel processing, large scale multimillion atom simulations with many-body potentials have become feasible.[11]

From an experimental point of view, fracture in ductile materials at a microscopic length scale and the role of defects is an interesting problem. It has been studied in copper containing a grain boundary.[12–14] Typically, a crack initiates at grain boundaries and propagates when microscopic cracks coalesce.

In this work we study crack initiation and propagation in copper with defects using a realistic many-atom, but now *ab initio* type, potential obtained from the effective-medium theory. Unlike the simulations by Zhou *et al.*[11]—done practically at zero temperature—we have studied the system also at room temperature. Previously,[15] we found that this potential gives reliable values for the elastic constants at room temperature for systems greater than $10^5$ atoms. We have checked that this is the case near zero temperature, too. In addition, the strength of the system and its size dependence were found to be in agreement both with experiments and simulations done with the empirical embedded atom model (EAM).

## II. POTENTIAL MODEL

In our model the interactions between copper atoms are described by the effective-medium theory (EMT),[16] which is an approximate method of calculating the total energy of an arbitrary arrangement of metal atoms from their spatial positions. EMT has been shown to be a powerful scheme for describing various bulk and surface properties of metals, such as thermal expansion and bulk melting,[18,17] defect energies,[19] dislocations,[20] surface relaxation and reconstructions,[21] surface melting[22] and roughening,[23] and also metal-impurity systems[24] and small clusters.[25] The many-atom nature of metallic cohesion is crucial in most of

 

these problems, which is the point where EMT has a clear advantage over the classical pair potentials. Compared to other many-atom potentials for metals, EMT has the strongest *ab initio* nature, since, in principle, all the parameters needed in the total-energy expression can be calculated using the jellium model and density-functional theory with the local-density approximation.[26] Other models (e.g., EAM), while resulting in a similar functional form for the total energy, are usually constructed in a more empirical way.

The central idea in the EMT formalism is to calculate the total energy of a system consisting of $N$ metal atoms

$$E=\sum_{i}^{N} E_C(\overline{n_i})+E_{AS}, \tag{1}$$

where the first term is the sum of individual ''embedding energies'' $E_C(\overline{n_i})$ depending on the spherically averaged background density $\overline{n_i}$ at the atomic site $i$. The radius of the ''atomic sphere'' $i$ is chosen such that the electron density in the sphere cancels the nuclear charge. This approximation is sufficient for calculating the basic cohesive properties of close-packed simple metal lattices at temperature $T=0$.[16] However, for finite-temperature studies and for systems with a more open lattice structure, the atomic sphere correction term $E_{AS}$ is needed to take into account the overlaps and neglected interstitial volume of the atomic spheres. This term defines largely the bulk elastic properties.

In the present work we use a modification of the original EMT scheme to extend the atomic interactions over three nearest neighbors of the fcc lattice.[18] This has been shown to improve the molecular-dynamics simulation results for several thermodynamic quantities and defect energies.[18–20] For details of the potential we refer to Ref. 18.

## III. LOADING SIMULATION

With the above potential model we have simulated failure under mode I and II loading using the molecular dynamics (MD's) (Ref. 27) method. In MD's the Newtonian equations of motion are numerically solved using (in this case) the velocity Verlet algorithm as the time integrator.[27] Initially, the atoms were arranged to form the fcc lattice and small Gaussian random deviations were added to the atomic coordinates. In addition, the initial velocities of atoms were selected from the finite-temperature Maxwell distribution. Furthermore, disorder was introduced to the system as point defects (vacancies and interstitials), as a grain boundary or as a small void to serve as seed for crack propagation. Vacancies were generated by removing randomly some atoms from the system and interstitials were generated by adding some atoms to random locations. In the case of interstitials, a threshold distance was needed (i.e., two atoms must not be too close to each other), since the potential is stiff, i.e., the initial forces can become unphysically large if no such threshold is used. Before starting the actual simulations the system was let to relax by thermalizing it with a Nose-Hoover thermostat[28,29] acting on the whole system for $6-12$ ps ($\approx 700-1400$ time steps) depending on the amount of initial defects.

In the tensile mode I test the fixed boundaries were moved apart vertically using the initially time-dependent strain rate

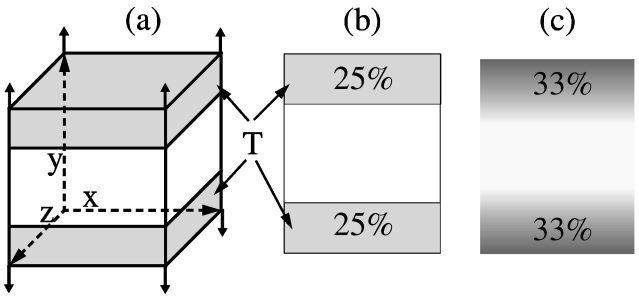


FIG. 1. The test setup for simulation (a) together with the previous (b) and the present (c) temperature control schemes. The thermostat ($T$) controls the temperature of the shaded regions, and the level of shading indicates the strength of coupling. In (b) the boundary between the regions in contact and not in contact with the thermostat could cause some problems (cf. text). Such boundary effects were avoided with scheme (c).

$\dot{\epsilon}\sigma(t,t_0,\alpha)$ [Fig. 1(a)]. Here $\dot{\epsilon}$ represents the maximum strain rate and $\sigma(t,t_0,\alpha)$ describes the smooth transition from the time-dependent rate to a constant rate. This sigmoid function was chosen such that $\sigma(t,t_0,\alpha)=(1+e^{\alpha(t-t_0)})^{-1}$, where $t$ is time and the parameter $\alpha$ determines the maximum acceleration ($=-\dot{\epsilon}\alpha/4$) occurring at time $t_0$. These parameters were selected such that $t_0$ is the time in which an elastic wave from the fixed boundary can propagate back and forth in the system in order to make the low and high amplitude waves interfere, and $\alpha<0$ was selected such that the boundaries reached 99% of the maximum velocity in $2t_0$. For the maximum strain rate we took $\dot{\epsilon}=113\%/\text{ns}$. For typical system sizes this strain rate corresponds to a displacement rate of the order $2\times10^{-3}c_l$, where $c_l$ is the longitudinal speed of sound in copper. This strain rate is a few orders of magnitude larger than the rate used in laboratory experiments, but much less than the speed of sound, cf. the recent discussion by Holland and Marder.[30] When the system was strained, its middle part (process region) was not in contact with the thermostat.

## IV. TEMPERATURE CONTROL

In our previous study[15] we controlled the temperature with a Nosé-Hoover chain[31] and during elongation only half of the system (atoms near the fixed boundaries) were in contact with the thermostat [Fig. 1(b)]. In that study we did not encounter problems, since either we had a homogeneous system, where a crack did not propagate, or we had a seed for crack propagation from which the crack initiated. However, when defects were introduced, but without introducing a seed for crack into the system, crack initiation occurred often near the boundary between the region in contact and not in contact with the thermostat (Fig. 2). To minimize the possible disturbance of this boundary on crack initiation, the temperature must be controlled such that the boundaries are fully in contact with the thermostat, but the process region of a propagating crack (middle part) is not in contact. In addition, the regions between these two regions are set in monotonically varying contact with the thermostat as shown in Fig. 1(c). This kind of temperature control has been proposed by Nosé[32] and we have chosen to use it here. In the Appendix we describe in detail the equations of motion of such a

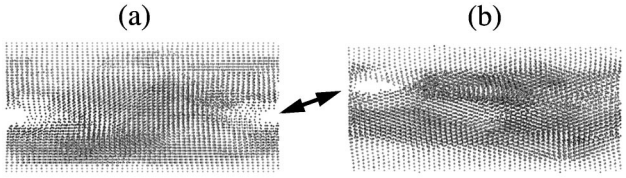


FIG. 2. Crack initiation in a system with the (vertical) straining direction being either along the [111] (a) or [011] (b) crystal orientation. Initially, 10% interstitials were generated into the system. When the system broke, crack initiation was seen near the boundary between the regions in contact and not in contact with the thermostat [cf. Fig. 1(b)]. Since such a boundary can cause crack initiation, the simulation setup is changed to avoid it.

gradual thermostat and how to choose its time scale parameter, $Q$. This parameter determines the characteristic frequency of the thermostat and we chose it to be one fifth of the characteristic frequency of thermal vibrations in copper (cf. Appendix).

This thermostat could control the temperature well up to the point of fracture. Then heat generation in the process region became so large that the temperature of the whole system started to increase rapidly. In Fig. 3 we show the internal temperature of the whole system and the weighed average temperature of the boundaries used in the controlling scheme [cf. Eq. (A10)]:

$$T_{int,bndry}=\frac{\Sigma_{j=1}^{N} f(\vec{q}_j)[\vec{p}_j\cdot\vec{p}_j/m_i]}{dk\Sigma_{j=1}^{N} f(\vec{q}_j)}. \tag{2}$$

In the system with 5% interstitials after initial thermalization, there is an increase in the initial temperature. However, the thermostat adjusts the temperature of the whole system near to the external temperature $T=10$ K and keeps the weighed average temperature of the boundaries practically the same as the external temperature. When the system fails, its structure changes and heat is generated into the system very rapidly. This heat is conducted to the region in contact with the thermostat, causing the internal temperature to decrease as depicted in Fig. 3.

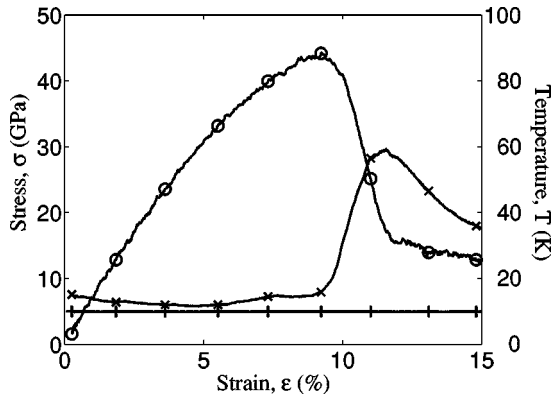


FIG. 3. Internal temperature of the system (×) and of the boundaries (+) as calculated using Eq. (2). The external temperature was $T=10$ K. An increase in the internal temperature is seen as soon as the system fails, i.e., the stress (○) decreases rapidly. Initially, the internal temperature is somewhat greater than the external temperature due to 5% random interstitials and their configurational relaxation.

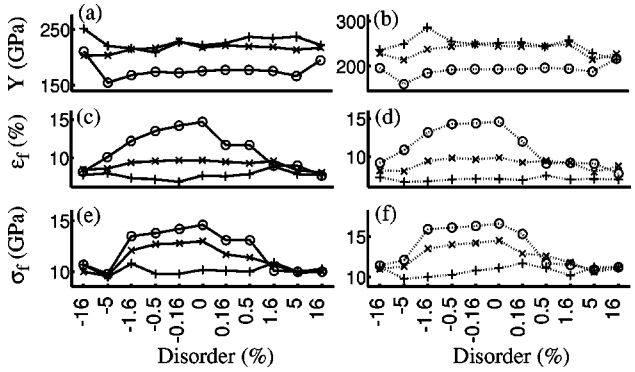


FIG. 4. (a),(b) Tensile modulus, (c),(d) fracture strain and (e),(f) fracture stress as functions of disorder. The amount of disorder is the number of interstitials divided by the initial number of atoms (%). Values less than zero denote the number of vacancies. Solid lines (a),(c),(e) and dotted lines (b),(d),(f) are the results at $T=293$ K and $T=10$ K, respectively. The system was elongated along the [010] (○), [011] (×), or [111] (+) crystal orientation.

## V. RESULTS

### A. Point defects

First we studied the strength and modulus of copper, where defects were introduced as vacancies or interstitials. In the case of vacancies, we removed atoms at random from the perfect fcc structure. In the case of interstitials, we added atoms at random to the perfect fcc structure such that two atoms were not too close to each other. We studied the cases where the number (proportional to the initial number of atoms $N\approx 1.3\times 10^5$) of interstitials or vacancies was 0, 0.16, 0.5, 1.6, 5, or 16%. The simulations were done both at room temperature ($T=293$ K) and near zero temperature ($T=10$ K). Before loading these systems were let to relax by initial thermalization as described above. The system with periodic boundaries was elongated in different crystal orientations, $y=[010]$, $y=[011]$, and $y=[111]$, the other orientations being $x=[100]$, $x=[01\bar{1}]$, and $x=[2\bar{1}\bar{1}]$, respectively, (and $\vec{z}=\vec{x}\times\vec{y}$). The results are depicted in Fig. 4.

It is seen from Fig. 4 that the increasing amount of defects will decrease the system strength both in terms of fracture stress and fracture strain. This tendency is most clearly seen in the case $y=[100]$. From Fig. 4 it is seen that interstitials decrease the system strength more effectively than vacancies. From Fig. 4 another interesting feature is evident: highly disordered systems, i.e., systems with a large number of defects are isotropic in terms of fracture stress or strain. In the case of $y=[111]$, the system strength in the ordered case almost equals the isotropic value, and thus in that case the strength is almost unaltered by this kind of disorder.

In addition, the tensile modulus does not change much with this disorder, and for a small amount of defects it seems to decrease with an increasing number of them. However, for $y=[010]$, the modulus of highly disordered systems is much greater than that of ordered systems. This can be due to the isotropic behavior of systems with a large number of defects.

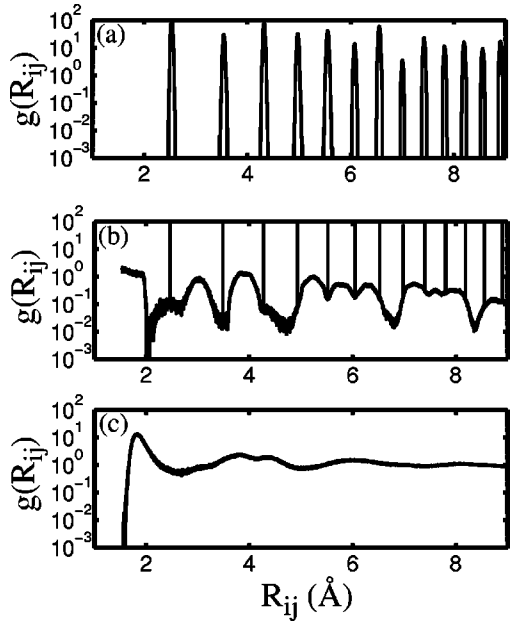


FIG. 5. Pair correlation functions: (a) of an ordered system after thermalization, (b) of a system with 16% interstitials before thermalization, and (c) of the same system as (b) after thermalization. In the highly defected case the initial crystal structure apparent in (a) and (b) is lost during thermalization in (c). The $y$ direction (free during the thermalization and fixed by loading thereafter) is [010] in all these cases.

Since the modulus for the [010] crystal orientation is the smallest, it should increase when the system becomes isotropic. Landau and Lifshitz[33] explain the isotropy of (poly-)crystalline materials (e.g., copper) with grains as follows. When the grains are small compared to the interesting length scale, the system consists of many randomly oriented crystallites, resulting in isotropic macroscopic properties. In these calculations we did not generate grains into the systems, but the random microstructure generated by defects should explain the isotropic behavior.

In addition to the isotropy due to the polycrystalline structure, a sufficiently large amount of vacancies might result in free-rotating grains, which in part can contribute to the isotropic behavior. However, in the case of interstitials we ought to note that the system is thermalized and that during the thermalization the structure of the system changes. In order to quantify these changes we show three different pair correlation functions (cf., e.g., Ref. 34). In Fig. 5 it is seen that a large number of interstitials can change the structure of the system drastically. In Fig. 5(c) there is hardly any sign of a crystal structure as compared to the ordered case after thermalization or the defected case prior to thermalization [Figs. 5(a) and 5(b), respectively]. Thus it is somewhat misleading to classify this case as being $y=[010]$ with defects. However, since this is the case prior to thermalization, we have used it throughout.

### B. Grain boundaries

In order to study the effect of grain boundaries, we introduced one such boundary between two grains with different crystal orientations. Then the system was allowed to thermalize to a given external temperature. As a first case, we studied a combination of two previously studied geometries, i.e., $y=[010]$ and $y=[011]$, corresponding to a boundary with a 45° tilt. This was done because from our previous studies we know the tensile modulus and fracture stress in both parts of the system, so that we can study the effect of grain boundary on these quantities. For these quantities in room temperature cf. Ref. 15.

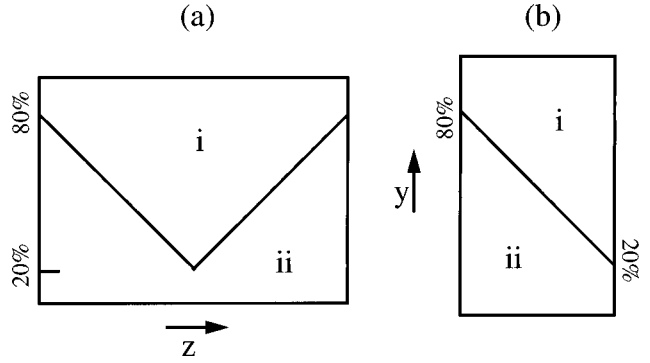


FIG. 6. The system with a 45° tilted grain boundary where the vertical boundaries are periodic (a) or free (b). Unless otherwise specified, the crystal orientations in the two regions are (i): $y=[011]$ against $x=[100]$ or (ii): $y=[010]$, against $x=[100]$. Tensile loading was applied in the $y$ direction, while shear loading was applied in the $x$ direction.

In the simulation, the $y$ boundary was fixed by loading and the other boundaries were free or periodic. In the case of free boundaries, one plane determined the grain boundary. However, in the case of periodic boundaries, two planes were needed to determine the grain boundary (corresponding to an infinite ''sawtooth'' grain boundary), cf. Fig. 6. With this geometry we performed tensile and shear tests with free and fixed boundaries. Initially, the system was thermalized to a low external temperature ($T=10$ K), after which the time was set to zero and straining was introduced as described above. During the initial thermalization phase the edges of the grain boundary tended to become smooth. However, at $t=0$ the straight parts of the boundary had affected the crystal structure of the individual grains and the potential energy of the atoms only very near the boundary (within $\approx 1$ lattice constant).

#### *1. Shear loading test*

In the case of shear loading, the system with fixed top and bottom boundaries and with otherwise periodic boundaries was sheared in the $x$ direction. This was done to determine the shear modulus that could be compared with our previous results $Y_{\perp,[010]}=81$ GPa and $Y_{\perp,[011]}=25$ GPa. These are the values obtained at $T=10$ K, for room-temperature values, see Ref. 15. It should be noted that the direction of shearing for each grain was selected as in our previous study, i.e., $y=[011]$ against $x=[01\bar{1}]$ for the top boundary and $y=[010]$ against $x=[100]$ for the bottom boundary movement. This is the only exception, where the crystal orientations given in the caption of Fig. 6 do not apply. From the simulation we obtained the modulus $Y_{\perp}=28$ GPa. Since this is between the two bulk values, we will analyze what the expected value for the modulus should be.

In order to do so we first consider a system of length $l$ that consists of parts of length $l_i$ and modulus $Y_i$ set in series, i.e.,

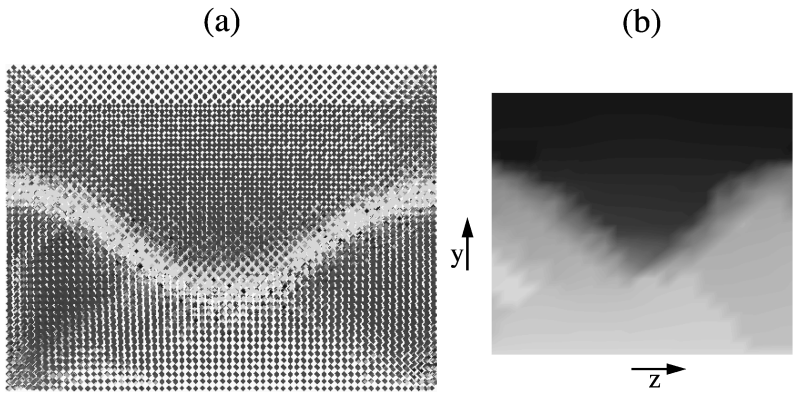


FIG. 7. (a) The potential energy shown as shading of the bulk atoms (i.e., boundaries excluded) at the end of the shear test. The grain boundary is the high-energy region. The smoothening during sliding is clearly seen (compare with Fig. 6). (b) Shape of the free boundary, and shading indicates the atom's $x$ coordinate. The region above the grain boundary has slided with respect to the region below the grain boundary. Sliding occurs at the grain boundary.

$l=\Sigma l_i$. A simple calculation shows that the total modulus $Y_s$ is

$$\frac{1}{Y_s}=\sum \frac{l_i}{l}\frac{1}{Y_i}. \tag{3}$$

In our case the system consists of three parts, two grains and the boundary between them. On the other hand, if these parts with the cross-sectional areas $A_i$ and moduli $Y_i$ are connected in parallel, the resulting modulus is simply the weighed average

$$Y_p=\sum \frac{A_i}{A}Y_i, \tag{4}$$

where $A=\Sigma A_i$ is the total area of the system. It is noted that this approximation does not take into account the coupling of the parts correctly, if they have different moduli at the same height. However, for our purposes it is a reasonable approximation. We assume that in the system the height of the grain boundary is $p_1 l$ (having the modulus $Y_1$) and the two grains can be described as slices in parallel, each slice having the grain heights $p_2 l$ and $p_3 l=(1-p_1-p_2)l$, where $p_2$ varies bilinearly (Fig. 6). Thus the distribution of $p_2$ is uniform between $p_l$ and $p_h$, and we expect the whole system to have a modulus

$$Y_{m,th}=\int_{p_l}^{p_h} Y_s \frac{dp}{(p_h-p_l)}. \tag{5}$$

Now if we assume that the grain boundary is thin, i.e., $p_1=0$, the geometry of the system determines that $p_l=0.2$ and $p_h=0.8$. Then the modulus of the system would be $Y_{\perp,th}=40$ GPa, which is significantly larger than the value obtained from simulations. Thus it seems that the grain boundary has a small shear modulus. In fact, if we assume a nonzero value for $p_1$ we can solve $Y_1$, which should be a reasonable approximation for the elastic modulus of the grain boundary. The height of the system was 27 lattice constants, which gives an approximation $p_1=5\%$ (since the structure of both grains was affected up to a distance of one lattice constant and the angle of the grain boundary is 45°). If half of the grain boundary belongs to both of the grains (i.e., $p_l=0.2-p_1/2$ and $p_h=0.8-p_1/2$), we can solve $Y_1$ from $Y_{\perp,th}=Y_\perp=28$ GPa giving $Y_1=4.4$ GPa. This analysis seems supported by the fact that from the atomic configuration we see most of the strain to concentrate near the grain boundary.

We have also sheared a system where the boundary perpendicular to the direction of shearing was free and the other boundaries were periodic (i.e., shearing of ''infinitely long'' sawtooth boundary). For symmetry reasons we took the direction of shearing to be $x=[100]$ in both the grains, cf. Fig. 6, not to be confused with the previous simulation geometry. When the system was sheared beyond the elastic limit, shearing resulted in sliding of the two grains with respect to each other, Fig. 7. In this sense the system is weakest at the grain boundary, since sliding occurred there. From Fig. 7 the rounding of the grain boundary edges is also seen as the straining increases. During sliding, the mean of the stress was seen to be constant, i.e., the system yielded plastically, Fig. 8(a). However, the stress had clearly an oscillatory form, with the period corresponding to a shear displacement of one half lattice constants. This is understandable since the {100} planes are located one half lattice constants from each other (cf. Ref. 35).

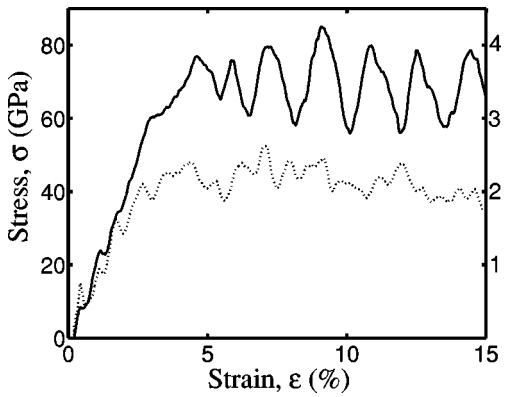


FIG. 8. Stress as a function of strain. (Solid line, scale on the left.) System under shear loading with free and periodic boundary conditions. The periodicity (1.8%) corresponds to one half lattice constants. (Dotted line, scale on the right.) System with free boundaries under tensile loading. The moduli differ from those given in text because of different boundary conditions.

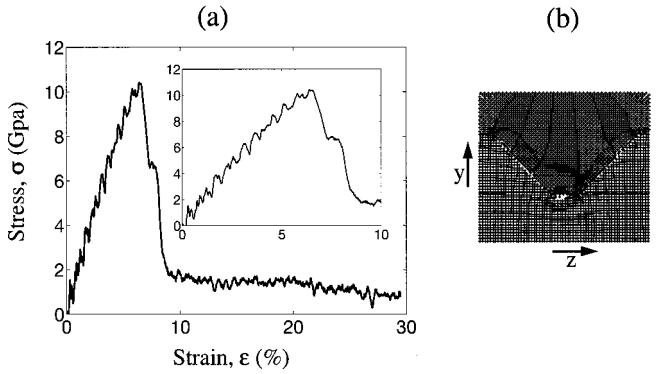


FIG. 9. (a) Stress as function of strain in a system with periodic boundaries including a grain boundary under tensile loading test. Most of the elastic energy of the system is consumed in crack propagation (strains 6.5% to 9.2%). (b) Atomic configuration of a thin slice (5 lattice constants) from the middle of the system when the strain is 6.5%. Crack initiation (i.e., a void) is seen at the center.

#### *2. Tensile loading test-periodic boundaries*

The tensile modulus was determined in the elastic region and we obtained the value $Y_{\parallel}=210$ GPa. This should be compared to the values for single crystal in our previous study: $Y_{[010],\parallel}=194$ and $Y_{[011],\parallel}=244$. If we once again use the above analysis scheme and assume that the grain boundary is infinitely thin, we would get $Y_{\parallel,th}=216$ GPa, which is more than the observed value. Thus the grain boundary should have a lower tensile modulus. More precisely, with the previous values of our geometry we get the tensile modulus of the grain boundary to be $Y_{GB,\parallel}=130$ GPa.

From an experimental study, Rabkin[36] concluded that the Young's modulus of the grain boundary should be one order of magnitude less the that of pure copper. The value we got for the tensile modulus of the grain boundary was only about 40% less than that of the whole system. It should be noted that the modulus depends on the thickness of the grain boundary, which was here 2 lattice constants and somewhat larger than in Rabkin's case. As a matter of fact, we could use in our analysis the experimental thickness for the grain boundary, $p_1=3.3\%$. With this we would obtain a value for the modulus that is about 50% of its bulks value, once again much larger than the value estimated by Rabkin. Thus these results are not in quantitative agreement with the experimental findings. However, it should be noted that the modulus of the grain boundary can crucially depend on its microstructure, which was not specified in the study cited.

In a very recent simulation by Schiøtz and co-workers,[37] it was found that the Young's modulus decreases as the number of atoms on the grain boundaries increase (i.e., the grain size decreases). This is in accordance with our results.

When the system was further elongated, it failed at the (macroscopic) strain of $\epsilon_f=6.5\%$, with the strength of the system being $\sigma_f=10.3$ GPa (cf. Fig. 9). In an ordered system with periodic boundaries we obtained the following orientation dependent strengths: $y=[010]$, $\epsilon_f=14.1\%$, $\sigma_f=14.5$ GPa and $y=[011]$, $\epsilon_f=10.8\%$, $\sigma_f=13.5$ GPa. Thus it is seen that both in terms of failure strain and stress the system with grain boundary is weaker than an ordered system. The failure mechanism in this case was crack initiation at the grain boundary, cf. Fig. 9. This is qualitatively in agreement with experiments,[13,14] where a crack initiates at the grain boundary and propagates along this boundary. Now an interesting question arises: is the fact that the system with this kind of disorder fails easier than an ordered system due to *lower local critical strain* or is the *modulus of the boundary* so much lower than the modulus of the grains that the local strain at the grain boundary exceeds the failure strain of the ordered systems? Because of nonlinearities in the stress-strain relation, this cannot be answered directly from the known $\sigma_f$ and $Y_{GB,\parallel}$. However, if we assume that in all the three regions $\epsilon_i/\epsilon_j=Y_j/Y_i$, we can solve the strain in each region from the total failure strain (in this case $\epsilon_f=6.5\%$). With this assumption the strain in the grain boundary can range between 7.7% and 8.9% corresponding to situations, where 17.5% or 77.5% (respectively) of the system has loading in the [011] orientation and the rest consist of the grain boundary (5%) and the other grain, where loading is in the [010] orientation. From Fig. 9 it is seen that fracture initiates at the location, where the increase in strain due to the difference of the moduli is highest. However, even there the strain, $\approx 9\%$, is not as high as the failure strain in an ordered system. Thus it seems that both these mechanisms affect the system failure at the grain boundary. This is interesting also in the context of the closely related bond or element models for highly disordered materials. In those models disorder can show in the local modulus[38,39] or in the rupture threshold,[40] but it seems that, at least in the case of paper, the latter is more realistic.[41] However, in the case of copper it seems that disorder affects *both* the local moduli and the local rupture threshold.

When the system was further elongated, crack propagation was observed. One might suspect that a crack should propagate perpendicular to the direction of straining. However, this was not the case and the crack was seen to favor the disordered region, namely, the grain boundary (cf. Fig. 10). This was also observed in experiments.[13,14] The crack was seen to propagate along the grain boundary almost through the whole system. However, at the strain of 9.2% the propagation ceased and the grains were in contact even at the total strain of 30%. From Fig. 9 it seen seen that in crack propagation most of the work done to the system prior to failure is consumed by crack formation (i.e., $\epsilon=6.5\%-9.2\%$). Thereafter the potential energy of the system is very low, and the crack grows only slowly, cf. Figs. 10(d)–10(f).

#### *3. Tensile loading test-free boundaries*

In our previous study, crack propagation was not seen in thick systems with free boundaries. This turned out to be the case also when a grain boundary was introduced to the system with free boundaries as depicted in Fig. 6. In this case the system failed at low strain and stress values, cf. Fig. 8. The failure strain is lower than the failure strain obtained in the ordered case $y=[010]$ ($\epsilon_f=7.5\%$, $\sigma_f=5.5$ GPa) but of the same order of magnitude as in the ordered case $y=[011]$ ($\epsilon_f=3.7\%$, $\sigma_f=4.0$ GPa). However, in the disordered case the failure stress, $\sigma_f$, was only 2.5 GPa due to the smaller tensile modulus. Thus, also the failure mechanism differed from that of the ordered case $y=[011]$ (where, in fact, slip planes were seen). In this case the failure occurred due to sliding of the two grains with respect to each other, cf.

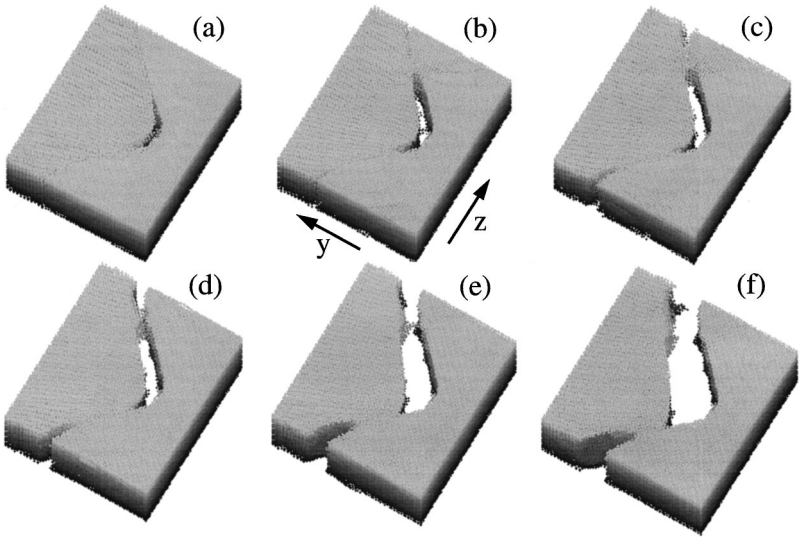


FIG. 10. Atomic configuration of the system when crack propagates. The strain in (a),(b)–(f) is 7.1, 8.0, 8.7, 8.2, 16, and 24%, respectively. The crack propagates along the grain boundary. When viewed as thin slices, it is seen that propagation is the result of coalescing voids. This can also be seen from (b), (c), and (d). Between (d) and (f) the crack grows very slowly.

Fig. 11. This kind of sliding was also seen in the studies by Schiøtz and co-workers.[37] Interestingly, during this sliding, the stress retained its value, i.e., the system yielded and the behavior was almost ideal elastic plastic [Fig. 8(b)].

### C. Large initial void

As a third type of defect, we studied how an initial seed for the crack affects the otherwise ordered system. With free boundaries a crack was not seen to propagate in a thick system and there we studied stress concentration and dislocation propagation. However, in thin systems crack propagation was seen.

#### *1. Stress concentration at crack tip*

First, we studied how the stress concentrates at the crack tip prior to plastic deformations. The initial void was made to the $x$ boundary, and we studied how the stress decreases as a function of distance from the crack tip. This was done by calculating the *local* microscopic stress tensor: $\vec{\vec{\pi}}_i$ (cf. Ref. 42)

$$(\Omega/N)\vec{\vec{\pi}}_i = m_i \vec{v}_i \vec{v}_i + \frac{1}{2}\sum_{j\neq i} \vec{F}_{ij}\vec{R}_{ij}\,. \tag{6}$$

Here $\Omega$ is the volume of the MD cell, $m_i$ and $\vec{v}_i$ are the mass and velocity of atom $i$, $\vec{F}_{ij}$ the force acting on atom $i$ due to atom $j$ as determined from the potential, and $\vec{R}_{ij}=\vec{r}_i-\vec{r}_j$ is the vector between atoms $i$ and $j$. It is clearly seen that the average of $\vec{\vec{\pi}}_i$ equals the stress, $\vec{\vec{\pi}}$ as defined in Ref. 42. Then we selected the atoms in front of the crack seed, perpendicular to straining, excluding boundaries, and averaged the local stress $\pi_i$ over $z$ and $y$ leaving us with the stress as a function of the distance from the crack tip. In Fig. 12 we show the maximum absolute value of principal stress as the function of the distance from the crack seed in the three geometries studied. It is noted that since the system is elongated, the stress is actually negative and thus the absolute value is shown. It seems that the inverse square-root dependence ($\sigma = K/\sqrt{2\pi r}$) Ref. 43 for the stress is not valid (here $r$ is the distance from crack tip). However, that result should hold only very close to the crack tip, since it is a first-order ap-

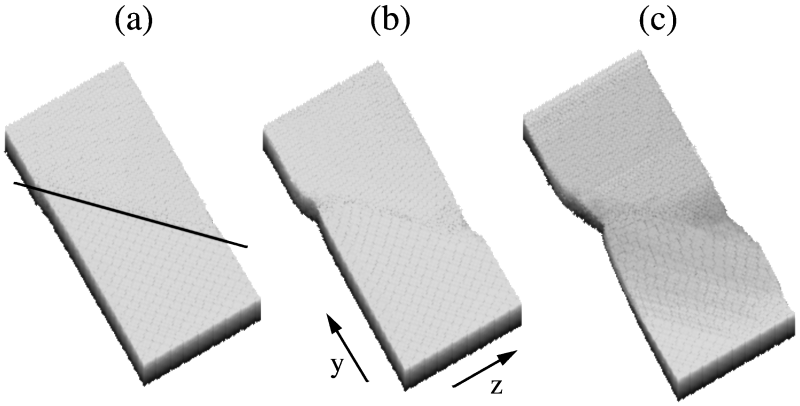


FIG. 11. Atomic configuration in a tensile test with free boundaries. In this case crack initiation or propagation is not seen. However, the grains slided with respect to each other. The strain (a), (b), and (c) is 3.3, 5.9, and 15%, respectively. The black line in (a) shows the location of the grain boundary.

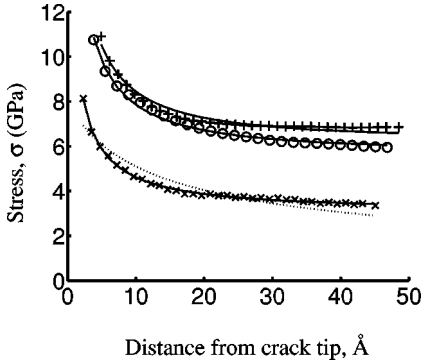


FIG. 12. Maximum principal stress as a function of distance from the crack tip. The solid lines stand for the scaling from Eq. (7) and seems to fit the data well. The dotted line is the inverse square-root scaling, which in this case does not apply. The different crystal orientations of loading are [010] (○), [011] (×), and [111] (+).

proximation for the case $r \ll a$, where $a$ is the crack width. In our case, the initial crack seed is not wide compared to the part of the system for which the above stress analysis can be made. Thus we should use the more accurate form[43]

$$\sigma = \frac{\sigma_{\inf}(r+a)}{\sqrt{r(r+2a)}}, \tag{7}$$

where $\sigma_{\inf}$ is the stress infinitely far away from the crack tip. From this form the inverse square-root dependence is obtained when $r$ is small compared to $a$, i.e., $r+a \approx a$. In Fig. 12 we show that this scaling agrees well with our calculations. It is striking to note that the continuum-based stress concentration seems to apply even at distances of the order of one lattice constant away from the crack tip.

#### *2. Dislocation propagation in thick systems*

When the system was further elongated, plastic deformation occurred in the form of slip planes. The present potential model gives a nice possibility to study the generation of these planes, i.e., dislocation propagation in the system, since the potential energy near the dislocation is greater than in the ordered bulk. This is depicted in Fig. 13, where two atomic

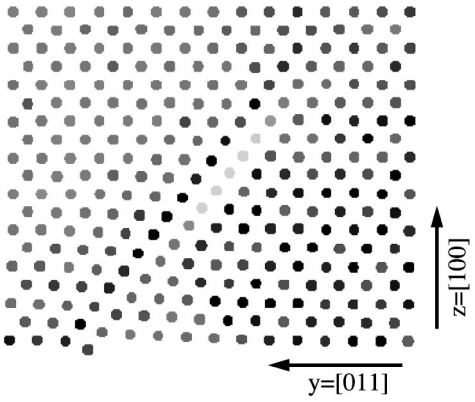


FIG. 13. Atomic configuration at the boundary of a propagating slip plane. Dark (light) atoms have low (high) potential energy. Two overlapping {110} atomic planes are shown. Dislocations are most visible when viewed from a low angle. The propagations of this boundary are depicted in Fig. 14.

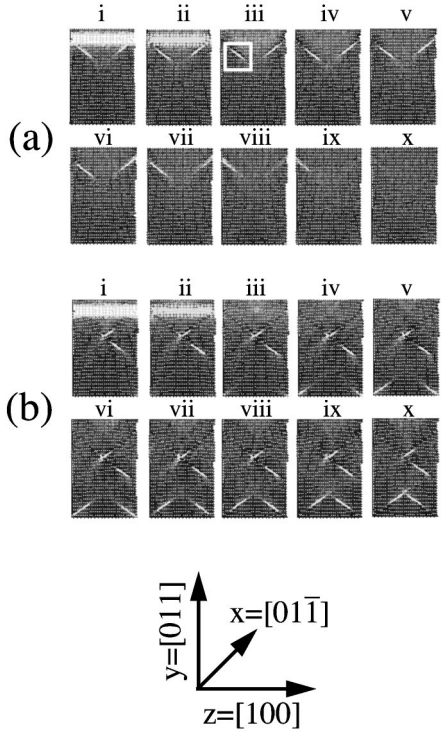


FIG. 14. Local potential energy of the system at two different time steps, $t=28.9$ ps (a) and $t=30.2$ ps (b). In each subfigure two atomic {110} layers are shown and the shading corresponds to the local potential energy of atoms. The $x$ coordinate increases with increasing subfigure number and subfigures $i$ are just in front of the crack seed. In the subfigures i and ii the stress (and energy) concentration are clearly shown. The white rectangular in a(iii) is shown in more detail in Fig. 13. The velocity of the slip plane in the $yz$ plane can be determined from these figures. From other similar figures its velocity in the $x$ direction was determined [cf. (a)$ix$-$x$.]

layers ({110} planes) are plotted together with the potential of the atoms.

From Fig. 14 it is seen how the slip plane forms. By keeping $x$ constant, we can determine the dislocation speed in the $zy$ plane, which is found to be 2710 m/s in the $[2\bar{1}\bar{1}]$ direction. On the other hand, we could determine the speed in the $x=[01\bar{1}]$ crystal orientation and found it to be 1600 m/s. To summarize, the plane seems to propagate in the $[10\bar{1}]$ crystal orientation with the speed of 3150 m/s. We studied also the other two geometries (cf. subsection V A), but there the boundaries affected the slip generation and its speed. However, the generation of {111} slip planes were observed in all cases.

The longitudinal and two differently polarized transverse speeds of an elastic wave in an anisotropic crystal can be solved from the dispersion relation (i.e., eigenvalue problem).[33] In the above crystal orientations the longitudinal and transverse wave speeds (subscripts $l$ and $t[\cdot]$ where $[\cdot]$ is the direction of polarization) for copper are as follows (in units of m/s):

$$[10\bar{1}]: c_l = 4960, \quad c_{t[010]} = 2900, \quad c_{t[101]} = 1620,$$

$$[\bar{2}11]: c_l = 5000, \quad c_{t[0\bar{1}\bar{1}]} = 2550, \quad c_{t[344]} = 2050.$$

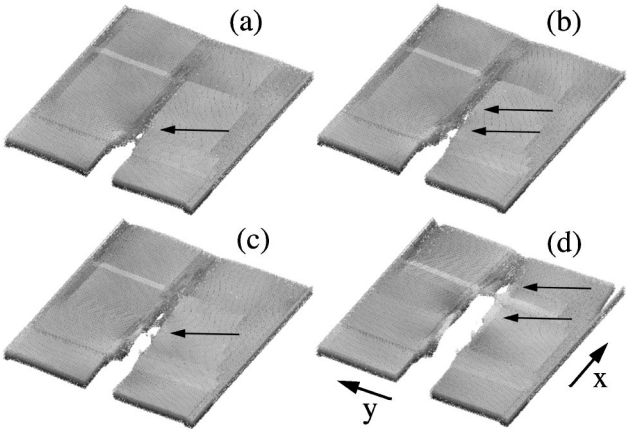


FIG. 15. The system with an initial crack seed elongated in the [011] crystal orientation ($y$), while the respective direction of crack propagation is [011] ($x$). The temperature was $T=10$ K. The system consists of $2\times10^5$ atoms and is only 3 lattice constants thick in the $z$ direction. The $z$ coordinate is shown as shading of the atoms. Free boundaries are used in both the $x$ and $z$ direction. Crack propagation is seen as a result of generation of microvoids and their coalescence. Total strain is 9.8 (a), 11 (b), 12 (c), and 17% (d).

Thus the speed of the dislocation forming the slip plane is roughly 60% of longitudinal wave speed, i.e., somewhat greater than the transverse wave speed.

It is interesting to note that the potential energy is concentrated just at the boundary of the propagating slip and that the size of this high-potential area does not change as the slip plane propagates, as is seen from Fig. 14. From Fig. 13 we can estimate the width of this boundary to be roughly 5 lattice constants and it seems to be just a plane, i.e., only the surface atoms of the unslipped part have high potential.

#### *3. Crack propagation in thin systems*

In the above thick systems with free boundaries we did not see crack propagation. However, when the system was made thin (three lattice constants in the $z$ direction) crack propagation was seen both with free and periodic boundaries. When this system was elongated in the [011] crystal orientation ($y$ direction) at $T=10$ K, crack propagation in the $[01\bar{1}]$ orientation ($x$ direction) was seen. Prior to rupture the process region became thinner and crack propagation was seen as a result of coalescing microvoids, cf. Fig. 15. This mechanism is typical for ductile fracture,[44] but, contrary to our simulations, microvoids are supposed to initiate near second phase particles, i.e., impurities. The crack was seen to propagate through the system with a velocity of $\approx630$ m/s. However, when the $z$ boundaries were periodic, crack arrest was seen. In that case a crack could propagate a short distance before its arrest and the speed was $\approx430$ m/s. In the literature several limiting crack speeds can be found.[45] These are determined in the isotropic and homogeneous continuum, which is a valid approximation for copper only at large length scales, when the microstructure is polycrystalline.[33] The most commonly cited limiting speed is by Roberts and Wells, $c_{rw}=0.38c_0$, where $c_0$ is the elastic bar wave speed, which depends on the Young's modulus ($E$) and density ($\rho$) of the system: $c_0=\sqrt{E/\rho}$. Other well-known theoretical limiting speeds are the Rayleigh speed $c_r=\chi c_2$ and the Yoffe limiting speed $c_y=0.6c_2$, where $c_2$ is the shear wave speed. It depends on the shear modulus $\mu$, which in turn is dependent on the Young's modulus and the Poisson ratio ($\nu$): $c_2=\sqrt{\mu/\rho}$, $\mu=E/2(1+\nu)$. The coefficient $\chi$ has a nontrivial[33] dependence on only the Poisson ratio. Substituting the values for copper[35] we get $\chi=0.935$ and then the above limiting speeds are $c_{rw}=1410$ m/s, $c_r=2020$ m/s, and $c_y=1360$ m/s. These values are all at least twice the speed we found in our simulation. It should be noted, however, that in our simulations crack propagation was the result of microvoid coalescence that has not been taken into account in the theoretical limiting speeds given above.

These thin systems or quasi-2D simulations were also done by setting $y=[010]$, $x=[100]$, and $y=[111]$, $x=[\bar{1}12]$. In the case $y=[010]$ the crack seemed to propagate in [110] and $[\bar{1}10]$ orientations giving further evidence that the $\langle110\rangle$ are somehow a preferred orientation for crack propagation. In the case $y=[111]$ the crack was seen to grow in the directions $\pm(2\vec{y}-\vec{x})=\pm[330]$ giving even further evidence of this preferred orientation. Originally, the preference for these crystal orientations was found by Abraham *et al.*[46] and they explained this to happen, since a crack seems to favor the *maximum* surface energy path.

Since the system is quasi-2D, we can expect that crack propagation is a result of slip generation, since the system becomes thinner and thinner while the slip occurs. If we assume that the system fails by reducing the area of the plastic neck[44] and that this reduction is due to the {111} slip planes, the direction in which the system should thin due to slipping is the direction in which the slip plane crosses the quasi 2D-system, i.e., the $xy$ plane. This direction is obtained as the cross product of the normals to the slip plane and the $xy$ plane. Thus the direction of crack propagation in these thin systems should be the cross product of the vector $[\pm1\ \pm1\pm1]$ and the vector $\pm\vec{z}$. In the first two loading cases, i.e., $y=[011]$ and $y=[010]$, this direction is one of the $\langle110\rangle$ orientations. In the case $y=[111]$, we have two possibilities, either the $\pm[110]$ orientations or the $\pm[\bar{1}12]$ orientations, of which the latter is parallel to $x$. Thus it seems that in the case of thin systems with free boundaries the slipping process plays a crucial role in crack propagation. However, in the last case the crack could have propagated also by slipping perpendicular to loading, which it did *not*. Furthermore, in our previous study[15] the $\langle110\rangle$ orientation was preferred by the crack even in thick systems with periodic boundaries. In that case, the preferred direction cannot be the result of the slipping process, making the system thin. Thus it seems that there is more to the preferred $\langle110\rangle$ orientations than just the slip making the system thin.

With periodic $z$ boundaries, crack propagation cannot be the result of slipping and thus thinning. We studied such systems at $T=10$ K. Even there a crack propagated in the $\langle110\rangle$ orientation for a short distance, after which it arrested. However, when the temperature was increased to $T=293$ K, no clear crack propagation was seen, only slow deformation and crack tip blunting. Thus there might exist a transition temperature in which the crack behavior in thin copper films would change. The results with periodic $z$ boundaries are somewhat similar for thick[15] and thin[47] sys-

tems. However, the behaviors are not identical, since in the case of a thin system with periodic boundaries crack initiation practically means that several close-spaced (in the periodic direction) microcracks initiate. In thick systems the spacing of these microcracks is much larger and thus the interaction of these cracks can result in different behavior in thick and thin systems with periodic boundaries. In Ref. 15 we saw that in a thick system with periodic boundaries the crack first formed a tube in the ⟨110⟩ orientation, while a neck could still carry a load. However, in thin systems these tubes (many due to the periodic boundary) are so close that no neck can be in between. Animations of these studies are available on the World Wide Web.[47]

## VI. SUMMARY

We have studied mechanical properties of copper using the molecular-dynamics method and the potential derived from the effective-medium theory. Three types of defects were studied: point defects, a grain boundary, and a larger void to serve as a seed for crack propagation. Simulations were done at room temperature or near zero temperature. The internal temperature of the system was controlled with a Nosé-Hoover thermostat that was in contact with the boundaries, but not in contact with the process region, and the boundary between these regions was smooth.

First we studied how interstitials and vacancies affect the tensile modulus and the strength of the system. The system strength in terms of fracture stress and strain was seen to decrease with an increasing number of defects. Contrary to ordered systems, the systems with a large number of defects appeared isotropic in terms of fracture stress and strain. Also, the tensile modulus decreased with the increasing amount of defects for a small number of interstitials or vacancies. However, due to the random microstructure, systems with a large number of defects appeared more isotropic than ordered systems in terms of the tensile modulus. Thus the tensile modulus in the [010] direction was, in fact, larger in the highly disordered case than in the ordered case.

Those systems that included a grain boundary were weaker than ordered systems in terms of the modulus, fracture stress, and fracture strain. In a shear test, the grains slided with respect to each other along the grain boundary, where the breakdown occurred. In a tensile test with periodic boundaries, a crack was seen to initiate at the point, where strain concentration due to the difference of the modulus of the grain boundary and the modulus of ordered bulk was largest. After initiation, the crack propagated along the grain boundary. These phenomena are in agreement with experiments done with copper. In our simulations we also observed microvoid coalescence as the mechanism for crack propagation.

In thick systems with free boundaries and an initial large void (i.e., crack seed) we studied stress concentration and {111} slip plane generation. The stress concentration was in agreement with continuum predictions even extremely close to the crack tip. Slip plane propagation was studied from the potential-energy distribution, which had a local maximum at the boundary of the propagating slip plane. The plane was seen to propagate in a ⟨110⟩ direction with a speed of about 60% of the longitudinal speed of sound for that specific crystal orientation.

When thin systems, including a crack seed and having free boundaries, were elongated, crack propagation was seen. In all cases, the crack propagated in the ⟨110⟩ crystal orientation by microvoid coalescence. We calculated the speed of the crack in the case, where the crack propagated perpendicular to loading. This speed, 630 m/s, was compared with some theoretical limiting speeds and it seems to be only 30% of the Rayleigh wave speed in copper.

Based on the high level of agreement with experimental data and on the results from the previous studies, we conclude that EMT molecular-dynamics simulations serve as a reliable and realistic tool for studying complicated mechanical processes in fcc metals.

## ACKNOWLEDGMENTS

This work has been financially supported by the Academy of Finland through the Matra and Graduate School programs and by the Jenny ja Antti Wihurin säätiö Foundation. Their support is greatly acknowledged.

## APPENDIX

In his review on constant-temperature molecular-dynamics methods, Nosé[32] very briefly proposed a scheme by which separate regions of the system can be in contact and not in contact with the thermostat, and the regions between these regions are in monotonically varying contact with the thermostat. It is instructive to derive these equations of motion, since this was not done in Ref. 32, and since this is fairly easily done by starting from a set of more general equations of motion proposed by Kusnezov and co-workers.[49]

When a $d$-dimensional system of $N$ atoms is simulated at a constant temperature $T$ with the original Nosé-Hoover (NH) thermostat[28,29] the equations of motion are as follows:

$$\dot{q}_i = \frac{p_i}{m_i}, \tag{A1}$$

$$\dot{p}_i = -\frac{\partial V(\vec{q})}{q_i} - \eta p_i, \tag{A2}$$

$$\dot{\eta} = \frac{1}{Q}\left[\left(\sum_{i=1}^{dN} \frac{p_i^2}{m_i}\right) - dNkT\right]. \tag{A3}$$

The parameter $Q$ can be introduced in Eqs. (A2) or (A3) and it defines the time scale of the thermostat $Q = dNkT\tau^2$, where $\tau$ is the characteristic time for the thermostat.[48,31] From Eq. (A2) it is seen how the inclusion of the thermostat modifies the Newton's equations of motion.

Kusnezov and co-workers[49] have proposed a generalization of the NH thermostat. They showed that the original Hamiltonian character of an ergodic system will be preserved with the following equations of motion:

$$\dot{q}_i = \frac{p_i}{m_i} - h_q(\eta_q) F_i(\vec{p},\vec{q}), \tag{A4}$$

$$\dot{p}_i = -\frac{\partial V(\vec{q})}{\partial q_i} - h_p(\eta_p) G_i(\vec{p},\vec{q}), \tag{A5}$$

$$\dot{\eta}_p = \alpha \sum_{i=1}^{dN} \left[ \frac{p_i}{m_i} G_i(\vec{p},\vec{q}) - kT \frac{\partial G_i(\vec{p},\vec{q})}{\partial p_i} \right], \tag{A6}$$

$$\dot{\eta}_q = \beta \sum_{i=1}^{dN} \left[ \frac{\partial V(\vec{q})}{\partial q_i} F_i(\vec{p},\vec{q}) - kT \frac{\partial F_i(\vec{p},\vec{q})}{\partial q_i} \right]. \tag{A7}$$

Here the temperature scale is different from that of Ref. 49 and therefore the Boltzmann constant has been introduced (cf. Ref. 32). The original NH equations of motion [Eqs. (A1), (A2), and (A3)] are obtained with the choices $F_i = h_q = 0$, $h_p(\eta_p) = \eta_p$, $G_i(\vec{p},\vec{q}) = p_i$, $\alpha = 1/Q$ and by defining $\eta = \eta_p$. Clearly, if the system consists of parts, where thermalization is not wanted, $G_i$ should be zero in such regions. We obtain a smooth change between the regions in contact and not in contact with the thermostat using a suitable choice of $G_i$. One such $G_i$ is $G_i(\vec{p},\vec{q}) = p_i f(\vec{q}_{j(i)})$, where $f(\vec{q}_j)$ is a smooth function of position that determines the coupling between a particle $j$ located at $\vec{q}_j$ and the heat bath, and $j(i)$ is the particle index, when the index $i$ of the generalized coordinate is known. Motivated by the original NH scheme, we take $0 \leqslant f(\vec{q}) \leqslant 1$. The other functions are selected as in the standard NH. Thus the NH-type equations of motion allowing smooth temperature control are[32]

$$\dot{\vec{q}}_j = \frac{\vec{p}_j}{m_j}, \tag{A8}$$

$$\dot{\vec{p}}_j = -\nabla_{\vec{q}_j} V(\vec{q}) - \vec{p}_j f(\vec{q}_j)\, \eta, \tag{A9}$$

$$\dot{\eta} = \frac{1}{Q} \sum_{j=1}^{N} \left\{ f(\vec{q}_j) \left[ \frac{\vec{p}_j \cdot \vec{p}_j}{m_i} - dkT \right] \right\}. \tag{A10}$$

Here $-\nabla_{\vec{q}_j} V$ is the force acting on particle $j$. We have used a piecewise linear $f(\vec{q})$ that decreases linearly from 1 at the boundary to 0 at one third and at two thirds the height of the system [Fig. 1(c)].

The dependence of $Q$ on $f^2$ can be fairly easily seen by defining an alternative thermostat variable $\eta_2 = \sqrt{Q}\,\eta$. Then the equations of motion read as follows:

$$\dot{\vec{p}}_j = -\nabla_{\vec{q}_j} V(\vec{q}) - \vec{p}_j \frac{f(\vec{q}_j)}{\sqrt{Q}} \eta_2, \tag{A11}$$

$$\dot{\eta}_2 = \frac{1}{\sqrt{Q}} \sum_{i=j}^{N} \left\{ f(\vec{q}_j) \left[ \frac{\vec{p}_j \cdot \vec{p}_j}{m_i} - dkT \right] \right\}. \tag{A12}$$

Thus it is seen that if $f$ is multiplied with a constant $\alpha$ and the parameter $Q$ with a constant $\alpha^2$, the equations of motion remain unchanged.

Following the argumentation of Toxvaerd and Olsen[48] [by differentiation of Eq. (A10) and in this case also by assuming only small movements of atoms and a slowly varying function $f(\vec{q})$, i.e., constant $f(\vec{q}_j)$ for each particle $j$] we have for the characteristic frequency of the thermostat

$$\omega^2 = \frac{1}{Q} \sum_{j=1}^{N} 2 f^2(\vec{q}_j) dkT. \tag{A13}$$

We chose the parameter $Q$ such that this frequency was one fifth of the characteristic frequency of the thermal vibrations in copper.


[1] S. J. D. Cox and L. Paterson, Phys. Rev. B **40**, 4690 (1989).

[2] Y. Mori, K. Kaneko, and M. Wadati, J. Phys. Soc. Jpn. **50**, 1591 (1990); Y.-H. Taguchi, Mater. Sci. Eng., A **176**, 295 (1994); T. T. Rautiainen, M. J. Alava, and K. Kaski, Phys. Rev. E **51**, R2727 (1995).

[3] B. deCelis, A. S. Argon, and S. Yip, J. Appl. Phys. **54**, 4864 (1983).

[4] E. Y. Baiguzin, A. I. Melker, and A. I. Mikhailin, Phys. Status Solidi A **108**, 205 (1988); S. J. Zhou, P. S. Lomdahl, R. Thomson, and B. L. Holian, Phys. Rev. Lett. **76**, 2318 (1996).

[5] B. L. Holian, A. F. Voter, N. J. Wagner, R. J. Ravelo, S. P. Chen, W. G. Hoover, C. G. Hoover, J. E. Hammerberg, and T. D. Dontje, Phys. Rev. A **43**, 2655 (1991); N. J. Wagner, B. L. Holian, and A. F. Voter, *ibid.* **45**, 8457 (1992).

[6] F. F. Abraham, D. Brodbeck, R. A. Rafey, and W. E. Rudge, Phys. Rev. Lett. **73**, 272 (1994).

[7] K. Sieradzki, G. J. Dienes, A. Paskin, and B. Massoumzadeh, Acta Metall. **36**, 651 (1988).

[8] M. Marder and X. Liu, Phys. Rev. Lett. **71**, 2417 (1993).

[9] M. Doyama, Nucl. Instrum. Methods Phys. Res. B **102**, 107 (1995).

[10] Y. W. Zhang, T. C. Wang, and Q. H. Tang, Scr. Metall. Mater. **33**, 267 (1995).

[11] S. J. Zhou, D. M. Beazley, P. S. Lomdahl, and B. L. Holian, Phys. Rev. Lett. **78**, 479 (1997).

[12] R. R. Keller, J. M. Phelps, and D. T. Read, Mater. Sci. Eng., A **214**, 42 (1996).

[13] A. Vinogradov and S. Miura, Scr. Metall. Mater. **32**, 427 (1994).

[14] Y. M. Hu and Z. G. Wang, Scr. Mater. **35**, 1019 (1996).

[15] P. Heino, H. Häkkinen, and K. Kaski, Europhys. Lett. **41**, 273 (1998).

[16] K. W. Jacobsen, J. K. Nørskov, and M. J. Puska, Phys. Rev. B **35**, 7423 (1987); K. W. Jacobsen, Comments Condens. Matter Phys. **14**, 129 (1988).

[17] P. Stoltze, K. W. Jacobsen, and J. K. Nørskov, Phys. Rev. B **36**, 5035 (1987).

[18] H. Häkkinen and M. Manninen, J. Phys.: Condens. Matter **1**, 9765 (1989).

[19] H. Häkkinen and M. Manninen, Phys. Scr. **T33**, 210 (1990).

[20] H. Häkkinen, S. Mäkinen, and M. Manninen, Phys. Rev. B **41**, 12 441 (1990).

[21] K. W. Jacobsen and J. K. Nørskov, Phys. Rev. Lett. **60**, 2496 (1988).

[22] P. Stoltze, J. K. Nørskov, and U. Landman, Phys. Rev. Lett. **61**, 440 (1988); Surf. Sci. **220**, L693 (1989); H. Häkkinen and M. Manninen, Phys. Rev. B **46**, 1725 (1992).

[23] J. Merikoski, H. Häkkinen, M. Manninen, J. Timonen, and K. Kaski, Phys. Rev. Lett. **70**, 2451 (1993); Phys. Rev. B **49**, 4938 (1994).
[24] O. B. Christensen, P. Stoltze, K. W. Jacobsen, and J. K. Nørskov, Phys. Rev. B **41**, 12 413 (1990).
[25] O. B. Christensen, K. W. Jacobsen, J. K. Nørskov, and M. J. Manninen, Phys. Rev. Lett. **66**, 2219 (1991).
[26] M. J. Puska, R. M. Nieminen, and M. J. Manninen, Phys. Rev. B **24**, 3037 (1981).
[27] M. P. Allen and D. J. Tildesley, *Computer Simulation of Liquids* (Oxford University, New York, 1987).
[28] S. Nosé, J. Chem. Phys. **81**, 511 (1984).
[29] W. G. Hoover, Phys. Rev. A **31**, 1695 (1984).
[30] D. Holland and M. Marder, Phys. Rev. Lett. **80**, 746 (1998).
[31] G. J. Martyna, M. L. Klein, and M. Tuckerman, J. Chem. Phys. **97**, 2635 (1992).
[32] S. Nosé, Prog. Theor. Phys. Suppl. **103**, 1 (1991).
[33] L. D. Landau and E. M. Lifshitz, *Theory of Elasticity*, 3rd ed. (Pergamon, New York, 1986).
[34] A. Rahman, Phys. Rev. **136**, A405 (1964).
[35] A. H. Cottrell, *The Mechanical Properties of Matter* (Wiley, New York, 1964).
[36] E. I. Rabkin, Scr. Metall. Mater. **30**8, 1043 (1994).
[37] J. Schiøtz, F. D. DiTolla, and K. W. Jacobsen, Nature (London) **391**, 561 (1998); cf. also S. Yip, *ibid.* **391**, 532 (1998).
[38] P. Heino and K. Kaski, Phys. Rev. E **56**, 4364 (1997).
[39] M. J. Korteoja, A. Lukkarinen, K. Kaski, and K. Niskanen, Phys. Rev. E **51**, 1055 (1995).
[40] A. Hansen, E. L. Hinrichsen, and S. Roux, Phys. Rev. B **43**, 665 (1991).
[41] L. Salminen, M. Korteoja, M. Alava, and K. Niskanen (unpublished).
[42] M. Parrinello and A. Rahman, Phys. Rev. Lett. **45**, 1196 (1980).
[43] H. L. Ewalds and R. J. H. Wanhill, *Fracture Mechanics* (Arnold, London, 1985).
[44] P. F. Thomason, *Ductile Fracture of Metals* (Pergamon, New York, 1990).
[45] M. F. Kanninen and C. H. Popelar, *Advanced Fracture Mechanics* (Oxford University, New York, 1985).
[46] F. F. Abraham, D. Schneider, B. Land, D. Lifka, J. Skovira, J. Gerner. and M. Rosenkrantz, J. Mech. Phys. Solids **45**, 1461 (1997); F. F. Abraham, Phys. Rev. Lett. **77**, 869 (1996).
[47] http://www.lce.hut.fi/~pah/Work_demo.html
[48] S. Toxvaerd and O. H. Olsen, Phys. Scr. **T33**, 98 (1990).
[49] D. Kusnezov, A. Bulgac, and W. Bauer, Ann. Phys. (Leipzig) **204**, 155 (1990).